Astron. Astrophys. 227, 553–562 (1990)

ASTRONOMY AND ASTROPHYSICS

An OH survey of Orion South and GMC214–13

P. Jenniskens[1] **and J.G.A. Wouterloot**[2,*]

[1] Sterrewacht Leiden, P.O. Box 9513, NL–2300 RA Leiden, The Netherlands
[2] Max–Planck–Institut für Radioastronomie, Auf dem Hügel 69, D–5300 Bonn 1, Federal Republic of Germany

Received May 22, accepted August 25, 1989

Abstract. A low resolution large scale survey of *OH* main line emission is presented that covers Orion South and GMC214–13, the giant molecular cloud associated with MonR2. *OH* emission is detected down to the lowest contours in the ^{12}CO survey of the Columbia group (cf. Maddalena et al., 1986). An LTE approach gives a mass distribution in Orion South that is similar to that derived from ^{13}CO and H_2CO observations and differs from that of $W_{^{12}CO}$. Peaks in the ^{12}CO emission, coinciding with reflection nebulae, are found at depressions and strong gradients in the LTE *OH* column density distribution. The total mass of GMC214–13 is found to be $(3 \pm 1) \times 10^5 M_\odot$ and that of Orion South $(10 \pm 3) \times 10^4 M_\odot$. The molecular gas is distributed in long filaments, both in Orion and in Monoceros. The filaments have weak projected velocity gradients of 0.04 km/s pc. The much stronger velocity gradient in the northern part of Orion South (0.14 km/s pc) and the high mean densities found there, must have their origin in momentum input by shocks and stellar winds originating from the OB association. In GMC214–13 there is no OB association nor do we find a similar area of dense matter or a strong velocity gradient as observed in Orion South.

Key words: interstellar matter: individual molecular clouds – MonR2 – Orion – radio lines: *OH* – survey

1. Introduction

With the recent ^{12}CO surveys by the Columbia group (Kutner et al., 1977; Morris et al., 1980; Maddalena et al., 1986) some insight has been obtained into the large scale kinematic and spatial distribution of molecular gas associated with the star forming regions of Orion and Monoceros R2. The study of star formation requires a thorough knowledge of the physical state of the molecular gas in the different parts of the associated giant molecular clouds, which can be obtained by comparing maps of several molecules and transitions. Here we present fully sampled maps of the usually optically thin *OH* main line emission at 1665 and 1667 MHz.

Send offprint requests to: P. Jenniskens
* Present address: 1. Physikalisches Institut, Universität zu Köln, Zülpicher Strasse 77, D–5000 Köln 41, Federal Republic of Germany

If both main lines are measured, *OH* column densities can be derived from the antenna temperatures and their ratio, assuming local thermodynamic equilibrium (LTE), that is equal excitation temperatures for both main lines (Goss, 1968). If the assumption of LTE fails and in the case of optical depths close to zero, it is possible to estimate the *OH* column densities from our observations only if we assume a constant beam averaged excitation temperature for one of both lines (Mattila et al., 1979, see Sect. 3.1). Because the *OH* column densities and also the *OH* abundances derived from these column densities depend strongly on the assumptions made, their value is in the fact that the *OH* column densities correlate with visual extinction (e.g. Wouterloot and Habing, 1984), which is thought to be proportional to the total gas column density. Therefore the *OH* observations provide an independent check on the total gas column density (mass and mean density) estimates derived from other molecular line transitions. By comparing these observations, which is done in Sect. 3.2, the true mass and mean density enhancements can be recognized.

The survey covers most of the giant molecular cloud associated with MonR2, which we will refer to as *GMC214–13*, and the southern part of *GMC209–19*, the giant molecular cloud found in Orion. Though similar in extend and z–distance from the plane, these are very different star forming regions. In GMC209–19 many high–mass stars are formed, in GMC214–13 probably none. The Orion and MonR2 associations are separated by about 300 pc and are both about 180pc below the galactic plane, which is a rather large z–distance. MonR2 is a cluster of reflection nebulae caused by a small number of B stars. Such stars are still forming in the cloud. There are no O stars in this area. The giant molecular cloud Orion South is associated with Orion OB1, a cluster of massive stars that contains at least 299 stars of type earlier than A0 (Warren and Hesser, 1977). There are numerous recently formed low mass stars and there is evidence for ongoing massive star formation.

In Sect. 4 we will consider the spatial and kinematic distribution of matter in both regions, which must reflect the reason for the large individual differences in massive star forming efficiency. We will first describe the global features of the area that concern our study.

1.1. The Orion region

Figure 1 shows the location of dark and translucent clouds in the area, that we found from a visual inspection of the POSS

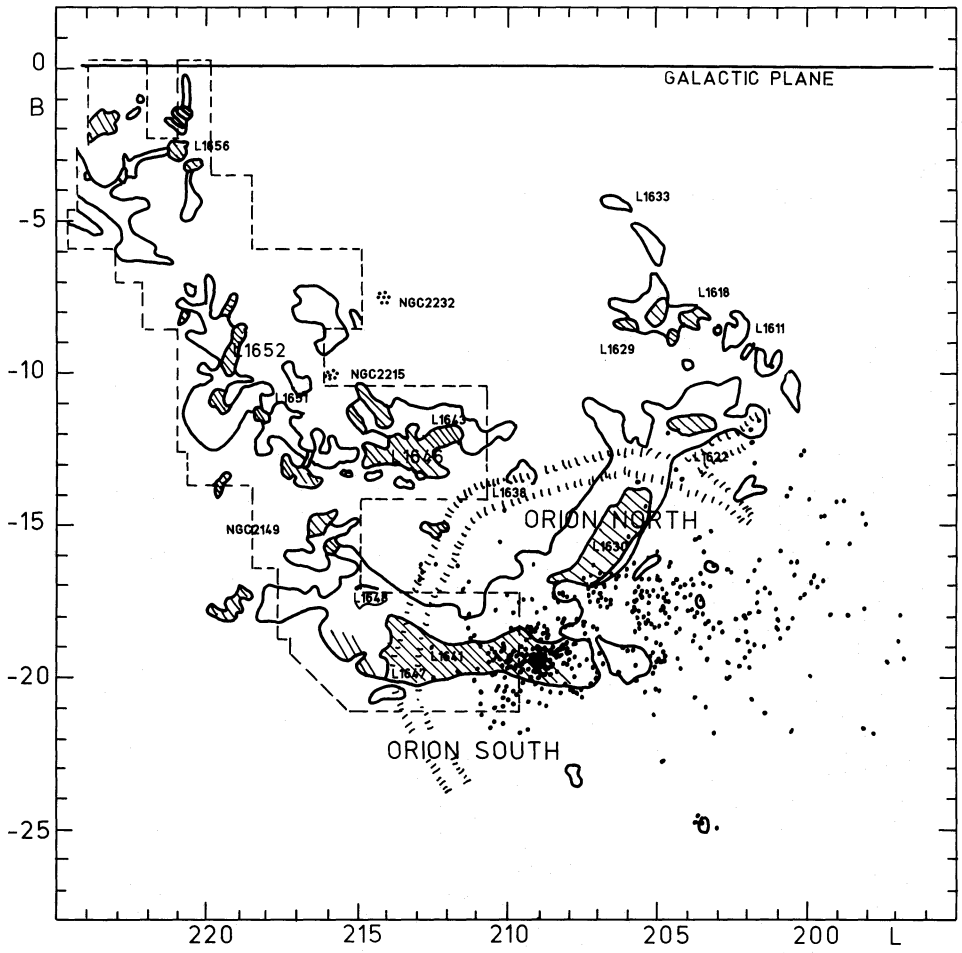

Fig. 1. The sky distribution of known Orion OB1 stars (dots, Warren and Hesser, 1977), the Barnard Loop and molecular clouds in the Orion and MonR2 regions, the latter from extinction features on the POSS plates. The dashed contour encloses the region that was searched for *OH* main line emission.

plates. The surveyed part is marked with dashed lines. Black dots show the position of OB stars that are members of Orion OB1 (Warren and Hesser, 1977).

One may compare the region of Orion in this two dimensional plot with Fig. 2, that schematically shows our impression of the most likely three dimensional structure of the Orion region. Open and filled circles represent the Orion OB1 stars. We have put a scale along the cluster to stress the distance spread among the stars. At the most distant point the stars are close to the molecular clouds Orion South (below) and Orion North (to the left). An HI shell surrounds part of the cloud and OB association. The position of the Sun is slightly below the (galactic) plane, shown left.

Orion North and Orion South are the main agglomerates of GMC209–19. Orion North is located in projection between the cluster and the galactic plane, and is elongated in a direction deviating by 45 degrees from a line of constant latitude. The northern part appears to be bent backwards from the association. The part facing the OB association, the front side, shows bright IR emission in the IRAS Skyflux maps (c. f. Israel, 1986) and there are many signs of low–mass star formation. The back side of the cloud has a veil of cirrus clouds.

Orion South is a large elongated molecular cloud, parallel to the galactic plane and almost in line with the OB association. In the best studied part of the cloud closest to the OB association an ∫–shaped ridge (OMC 1,2) is found (Bally et al., 1987), that contains molecular gas of high mean density and the bipolar outflow source IRC–2, probably a recently formed and still

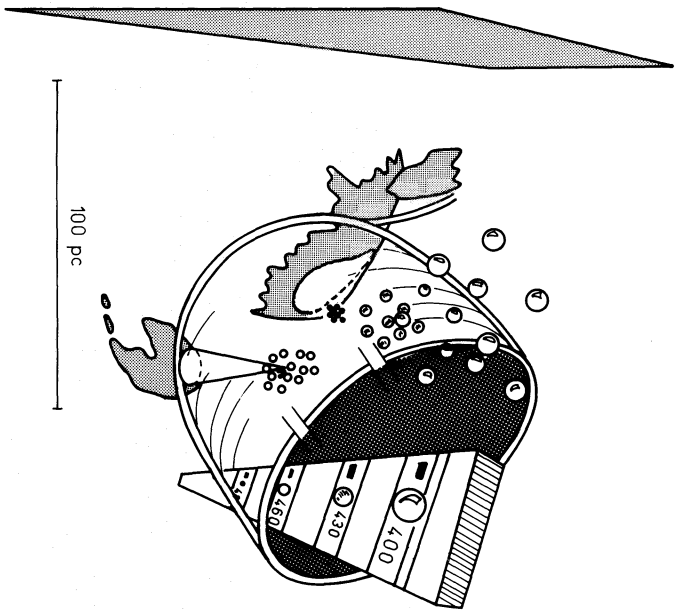

Fig. 2. A schematic picture of the three dimensional structure of the Orion Region. Open and filled circles represent the Orion OB1 stars. A scale put along the cluster stresses the distance spread among the stars. At the most distant point the stars are close to the molecular clouds Orion South and Orion North. An HI shell surrounds part of the clouds and OB association. The observer is put slightly below the galactic plane near the position of the Sun.

embedded high mass star (Downes et al., 1981; Zeng et al., 1987). The ridge is at the top of a *A*–shaped region with a small vertex angle. The whole structure with $L < 213^o$ resembles a shock front refracting around a high density inhomogeneity in the interstellar medium (Bally et al., 1987). If shocks from supernova explosions have sculpted the cloud, they probably originated in the OB assocation, suggesting that this part of the cloud is facing away from the cluster. The "cone" extends southwards, up to $L = 213^o$. The molecular gas on the edges of the cone is highly clumped. There are many signs of low–mass star formation: T–Tauri stars (Parsamian and Chavira, 1982) and IRAS point sources from cores and imbedded T–Tauri stars (Beichman,1986).

The Barnard Loop, shown by dashes in figure 1, is the ionised edge of an HI shell surrounding a giant hot bubble (Reynolds and Ogden, 1979; Cowie et al., 1979), caused by the input of energy and momentum from the (evolving) OB cluster (Castor et al., 1975). The shell is seen to extend to $B = -50^o$ and is expanding with 10–15 km/s. The mean velocity of expansion is slightly negative, which implies that the expansion has an effective component in our direction. As a result the (elongated) shell may be pointed towards us (Reynolds and Ogden, 1979). It is not clear if the gas outside the shell is the hot (10^6K) gas of a supernova dominated medium (McKee and Ostriker, 1977) or contains warm (10^4K) gas (Field et al., 1969). Only in the latter case does the shell indicate a real bubble. Cowie et al. (1979) found highly ionised gas at high negative velocities ($V_{lsr} \sim -100$ km/s) toward several stars located inside the bubble, which they interpreted as a radiative shock surrounding the shell (Orion's Cloak).

1.2. The Monoceros region

MonR2 is a group of relection nebulae at a distance of 830 ± 50 pc (Herbst and Racine, 1976). The nebulae are due to a group of B1–B6 stars in the molecular cloud *L1646*. At $L = 213^o.7$ and $B = -12^o.6$, in this cloud, there is a bipolar outflow source, possibly a young B0 star, and a cluster of IR sources (e.g. Downes et al., 1975). Unlike the Orion region, no O stars are associated with this star forming region. L1646 is part of a giant molecular cloud which we refer to as *GMC214–13*. The molecular gas is found at radial velocities of $8 - 16$ km/s.

A small part of this cloud complex is seen behind Orion South. The significant difference in radial velocity of this gas with respect to that of Orion South and the confinement of the gas in velocity space, makes it likely that this material is associated with the molecular cloud that is seen nearby in projection on the sky (Maddalena et al., 1986). In this cloud there are reflection nebulae, NGC2149 (= VdB 66) and VdB 64, with associated stars at distances of about 830pc and 790pc (Racine, 1968). This is roughly the distance of MonR2. Following Maddalena et al., we will refer to this cloud as *NGC2149*. South of L1646 is a third large cloud called L1652, that contains the reflection nebula VdB80 which surrounds a beautiful compact cluster of B3–A2 stars at $L = 219^o.3$, $B = -8^o.9$. The brightest star, of type B3ne, is at a similar distance of about 760pc (Racine, 1968).

2. Observations

2.1. Observing procedures

Between April and October 1984, in January 1985 and in October 1988, we obtained 1500 spectra of both *OH* main lines with the 25m Dwingeloo Radio Telescope (half power beam width 31', main beam efficiency 0.76). The 256 channel autocorrelation spectrometer was split into two equal parts, each recording the emission of one of the two lines. With a bandwidth of 625 kHz, the velocity resolution is 0.88 km/s. The total velocity coverage is 112 km/s, centered on $V_{lsr} = +10$ km/s. All velocities given are relative to the local standard of rest using a Standard Solar Motion of 20.0 km/s towards $L = 56^o.2$, $B = 22^o.8$.

Integration times were 30 minutes per grid point resulting in an rms noise level of 0.02K. Both the signal–to–noise ratio and the velocity resolution are a factor of 2 better than that of Baud and Wouterloot (1980). A grid of positions 0.3^o apart (shown by the dashed contour in Fig. 1), was completely sampled with the 0.52^o beam. The area surveyed covers Orion South, MonR2, L1652 and some clouds near L1656, and was selected using the early IRAS spline maps.

The total power mode was used with a reference spectrum taken at the equatorial North Pole ($L = 123^o.0$, $B = +27^o.4$). During the reduction we found weak asymmetric emission in the reference spectra at $V_r = -5.8 \pm 0.4$ km/s, with a large linewidth of 5.5 km/s and a peak temperature of 0.038 ± 0.004 K at 1667 MHz and 0.018 ± 0.004 K at 1665 MHz. The emission probably originates from local clouds along the line of sight. The IRAS Skyflux maps show 100 micron emission at this position; HI spectra of nearby positions show emission at a velocity of $V = -4.5 \pm 1.0$ km/s (Heiles and Habing, 1974; Weaver and Williams, 1974). According to Maddalena et al. (1986) there is no molecular line emission at these negative velocities in the region surveyed, so this weak signal in our reference spectra does not interfere with the observations.

Our temperature scale is in agreement with that of Baud and Wouterloot (1980). Note that all other split band (2×128 channels) observations obtained with the Dwingeloo Radio Telescope prior to 1988 have antenna temperatures that are a factor of two too low. These involve earlier publications by one of the authors (Wouterloot and Habing, 1984; Wouterloot 1984a, 1984b). The source of the factor two difference between the observations using 1×256 and 2×128 channels is unknown yet. In October 1988 we checked both temperature scales by a series of observations of line sources (*OH* 1612 and 1667 masers and molecular clouds) and found a difference of a factor of 1.9 ± 0.1 (Jenniskens, 1988). A comparison with literature data (Turner and Heiles, 1974; Cohen et al., 1983) showed that the temperature scale for unsplitted band observations is correct.

2.2. Observational results

From each spectrum a polynomial baseline of order 4 or less (usually of order 3) was subtracted interactively. Up to two out of six subscans were removed in case of interference, increasing the noise of some scans by 20%. Figure 3 shows the resulting peak antenna temperatures for the velocity range from 0 to +17 km/s. The 1665 MHz emission relative to that at 1667 MHz is strong for Orion South and weak for GMC214–13 ($B < -17^o$). The 1665 MHz line is significantly stronger than the 1667 MHz line only at $L = 213^o.7, B = -12^o.6$, where a type I OH maser is situated (Downes et al., 1975).

Figure 4 shows the integrated antenna temperature at 1667 MHz (W_{OH}, in K km/s), for the velocity interval of –0.1 to 8.7 km/s (mainly emission from GMC 209-19) and for 8.7 to 17.5 km/s (mainly emission from GMC 214–13). No significant emission was found from gas at velocities outside these intervals.

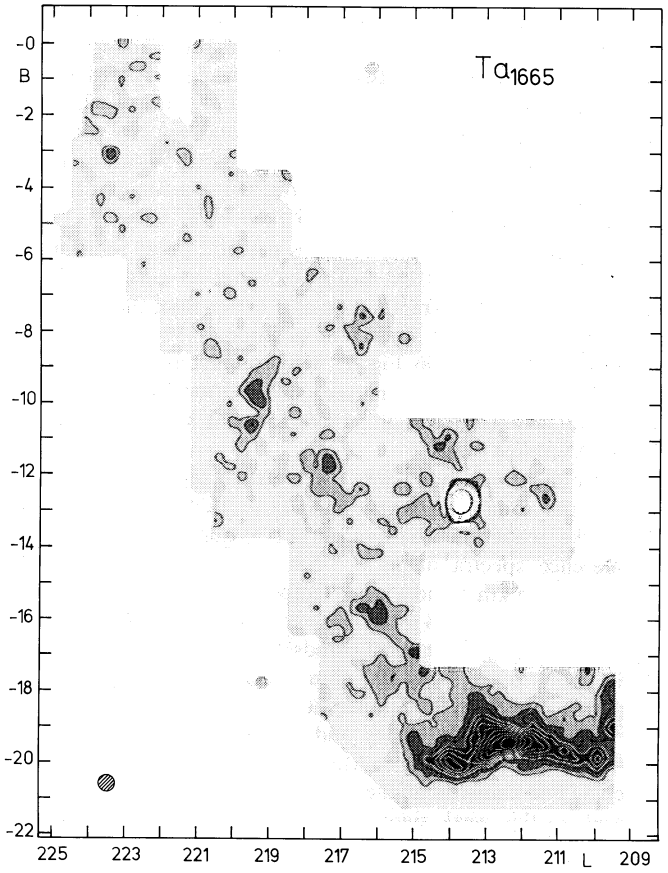

Fig. 3a. $L - B$ map of the 1665 MHz peak antenna temperature sky distribution. At $L = 213.7, B = -12.6$ a type I OH maser is found. Contour values: (0.06), 0.08, 0.12, 0.16, ... K.

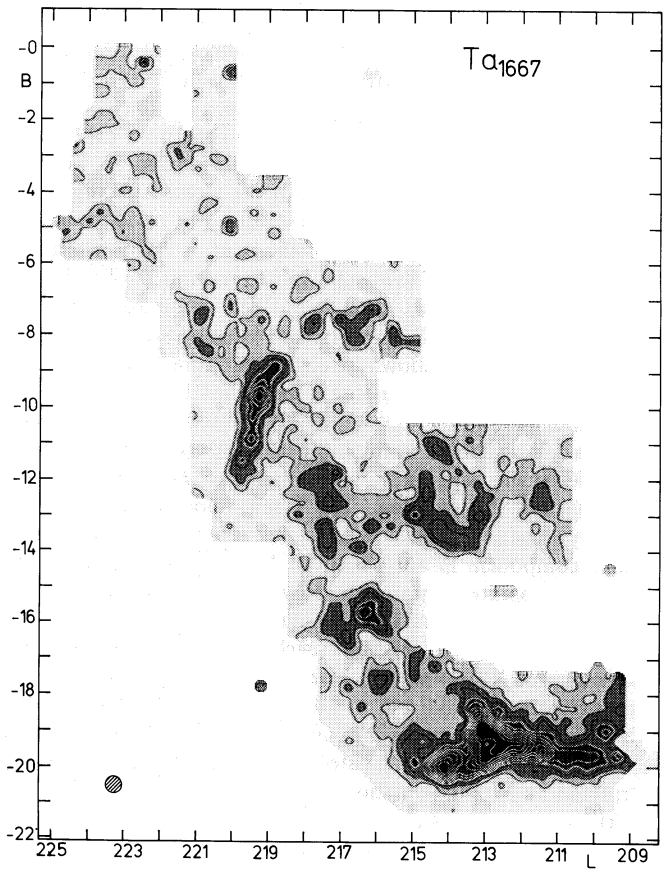

Fig. 3b. $L - B$ map of the 1667 MHz peak antenna temperature sky distribution. Contour values as in Fig. 3a.

1667 MHz emission is observed almost to the lowest (1.3 K.km/s) contour of the W_{CO} maps by Maddalena et al.. At a first glance the general agreement as to the location of molecular gas in the W_{OH} and W_{CO} data is striking.

The observed velocity field is similar to that found by Maddalena et al. (plate 1) from CO data. The distribution of linewidths is also similar to that of the ^{12}CO linewidths (plate 2, Maddalena et al.). The full width at half maximum (corrected for instrumental broadening) is found to be between 1.5 and 2.5 km/s, with a few exceptions in Orion South, near $L = 213^o.0$, $B = -19^o.5$ and for $L < 212^o.0$. This is the area of the cone. Here the linewidths are at some places as large as 4 km/s, probably as a result of the overlap of spatially separated cloud clumps in the line of sight at slightly different central velocities. The OH spectra show two peaks at some of these locations (Jenniskens et al., 1985).

3. Cloud masses and mean densities

3.1. Methods

The OH column density is calculated from (Goss, 1968):

$$N_{OH} = 2.386 \times 10^{14} T_{ex}(1667) \tau_{1667} LW_{1667} \qquad (1)$$

with T_{ex} the excitation temperature and LW the FWHM linewidth. The optical depth τ follows from the main line ratio and the equation of elementary radiation transfer in case of local thermodynamic equilibrium (LTE). LTE may however not aply. Small main line anomalies are caused by infrared pumping (Guibert et al., 1978; Bujarrabal and Nguyen-Q-Rieu, 1980) and ultra violet pumping with and without infrared line overlap (Crutcher, 1977; Bujarrabal and Nguyen-Q-Rieu, 1980) as for collisional excitation by electrons (Guibert et al., 1978), ions (Bouloy and Omont, 1977, 1979), H atoms (Kaplan and Shapiro, 1979) and H_2 molecules (Bertojo et al., 1976; Kaplan and Shapiro, 1979; Dixon and Field, 1979; Bujarrabal and Nguyen-Q-Rieu, 1980; Flower, 1980 – but also see Andresen, 1984, 1986). The importance of these mechanisms strongly depends on the local physical conditions. Small positive as well as negative excitation temperature differences are possible, resulting in a significant change of the main line ratio. The definition for the main line ratio (R) used in this article is:

$$R = \frac{T_a(1665)}{T_a(1667)} \qquad (2)$$

In LTE, R is expected to range from 0.55 (optically thin) to 1.0 (optically thick). Main line ratios in the center of the clouds are given in Table 1.

Values deviating significantly from the optically thin value are found in Orion South, except for the most southern part of this cloud. In the central areas R is about 0.7 ($\tau \simeq 1$). For $L < 212^o.7$ the main line ratios are higher even, on average

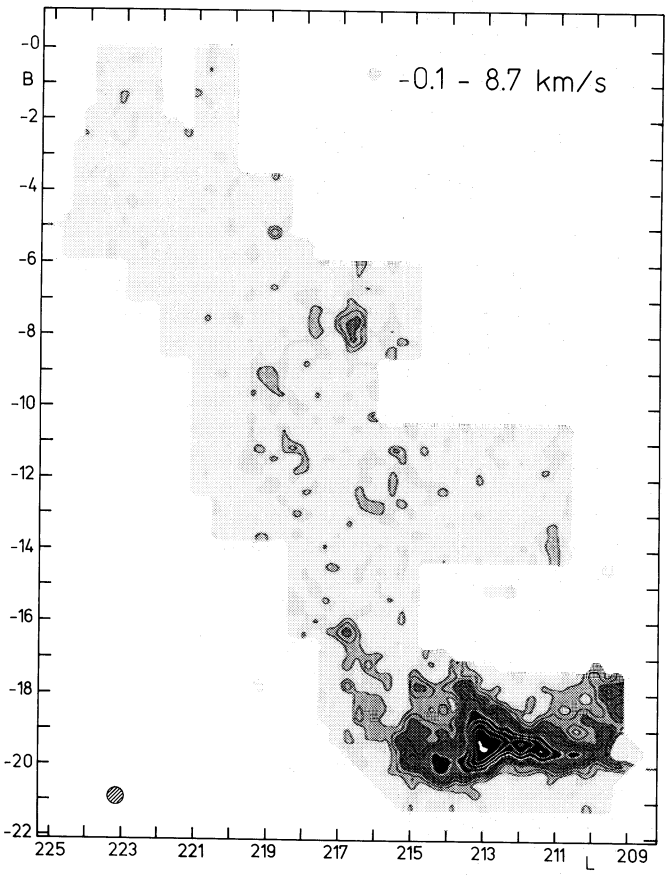

Fig. 4a. $L-B$ map of W_{OH}, the 1667 MHz emission integrated between velocity $-0.1 < V_r < 8.7$ km/s, which shows mainly the clouds of Orion South. Contour values: (0.1), 0.2, 0.3, 0.4, ... K.km/s.

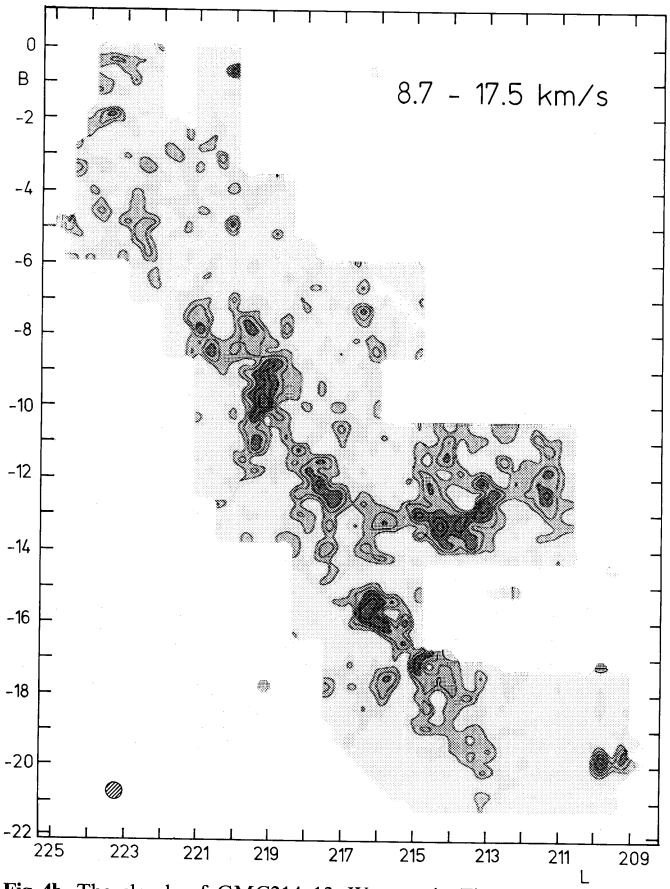

Fig. 4b. The clouds of GMC214–13. W_{OH} as in Fig. 4a, but for $8.7 < V_r < 17.5$ km/s.

about 0.87 ($\tau \simeq 3$), and close to M42 (at $L = 209^o$) main line ratios are as high as 1 at some locations.

High OH optical depths, as implied by the high main line ratios found, are not unexpected for this area. Orion South has to be abundant in dense cores because many low–mass stars are forming there. From a comparison of OH and H_2CO Cohen et al. (1983) concluded that the OH lines in Orion South are saturation–broadened by about 16%. This implies an optical depth of about 1 (somewhat less than derived from the main line ratio). Similar high main line ratios for high peak antenna temperatures are found in areas k and l in Taurus (see Wouterloot and Habing, 1984). For this region the LTE optical depth weakly correlates with photographic extinction (correlation coefficient 0.52). The OH fractional abundance, derived from LTE OH column densities assuming a beam filling factor of 1 and adopting the correct temperature scale as discussed in Sect. 2.1, is as high as $\frac{N_{OH}}{N_H} = (7 \pm 2)x10^{-7}$. Also in case of a general small increase of the main line ratio in dense clouds, this value will scale the 'LTE OH column densities' to reasonable total gas column densities if the beam filling factors in Orion South are not considerably less than those in Taurus area k and l.

OH column densities for Orion South were calculated for slightly smoothed main line ratios, obtained by applying a gaussian smoothing function of 0.5^o FWHM. All low signal-to-noise main line ratios with $0.07 < T_a(1667) < 0.1$ and $0.04 < T_a(1667) < 0.07$ K were averaged and set to the averaged values of 0.67 and 0.60 respectively. The main line ratios higher than 0.95 were set to 0.95 and those less than 0.56 were set to 0.56. The result is shown in Fig. 6b, and will be discussed in the next paragraph.

In L1646, and especially in L1652, the main line ratios tend to be very low for high antenna temperatures: $0.45 \pm 0.05(1\sigma)$, somewhat less than allowed for LTE. Figure 5 shows the main line ratio as a function of the inverse of the peak antenna temperature at 1667 MHz. Noise in both spectra tends to bring the ratios toward the value showed by a dashed line, which was derived from an empty part of the spectra, between $17 < V_r < 26$ km/s. All clouds of GMC214–13 tend to have ratios above the dashed line. This implies that the main line ratio of weak lines is high, above 0.8. The high main line ratios for weak lines and the lower than allowed (0.55) main line ratios for the strongest lines, point to small non-LTE effects influencing the main line ratios. Such non-LTE effects are known from previous work on diffuse molecular clouds (e.g. Crutcher, 1977; 1979). Background source observations of diffuse molecular clouds, with $A_v \sim 1$, give independent estimates of optical depths and excitation temperatures that appear to be between 0.01 and 0.1 and about 5.5K respectively (Dickey et al., 1981). For such low optical depths equation (1) may be rewritten as (Mattila et al., 1979):

$$N_{OH} = 2.242 \times 10^{14} f \frac{T_{ex}(1667)}{\eta F (T_{ex}(1667) - T_{bg})} W_{OH} \qquad (3)$$

where f corrects for the finite optical depth; f ranges from 1.0

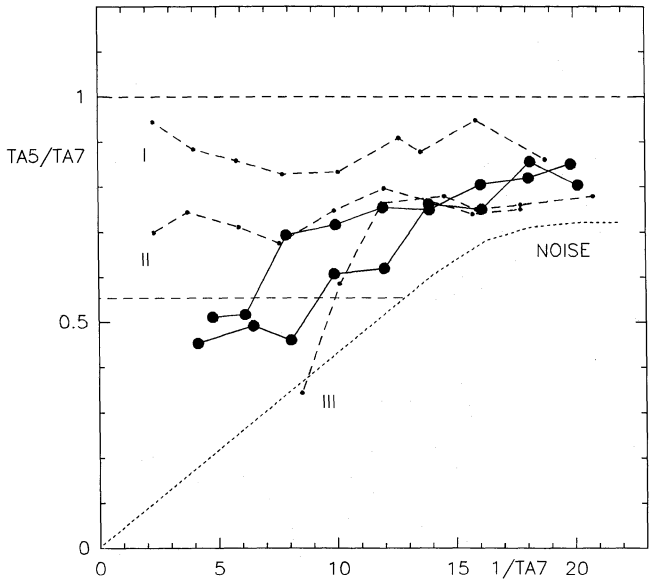

Fig. 5. The main line ratio ($\frac{Ta(1665)}{Ta(1667)}$) versus peak antenna temperature at 1667 MHz. Large dots are for GMC214–13: L1652 (below), L1643/51 and NGC2149 (above). Small dots are data for three areas in Orion South. I: $210.0 < L < 212.7$, II: $212.7 < L < 215.5$ and III: $215.5 < L < 217.5$. Dashed lines give the range of allowed values in case of LTE and the value expected if a large number of grid points are included in the averaging that contain noise only.

for $\tau << 1$ to 1.38 for $\tau = 1$; η is the beam efficiency and F the filling factor.

The background continuum emission (T_{bg}) in the Orion and Monoceros region is 3.1 ± 0.2 K at 18cm everwhere below $B = -5^o$ and about 3.4K near the galactic plane. The contribution from the foreground local emissivity, estimated to be only $0.14 \pm 0.05K$ (from Beuermann et al.,1985), has been subtracted. If the geometry sketched in Fig. 2 is correct, the continuum emission from the Barnard Loop (0.26 ± 0.05 K) is at least partly a foreground feature also. Its influence is negligible, less than about 10% on the OH column densities at the Loop's position. It cannot cause the peak in OH emission observed at $L = 213$.

For the areas with low OH optical depth, clumping is probably not important. F is assumed to be 1. Of course the OH column density distribution and the final mass estimates are not affected by F, only if F is constant in these and other local areas with low optical depth.

In case of main line ratios found close to the optical thin value, an alternative to the assumption of LTE is the assumption of a (beam averaged) constant excitation temperature, taken at $T_{ex}(1667) = 5.5$K. The OH column density calculated from Eq. 3 is proportional to W_{OH} (Fig. 4). The integrated W_{OH} value over the cloud area, including the outer boundaries, is given in Table 1. From this value a mass estimate may be derived, taking into account a number density of about 12% of helium atoms (following Maddalena et al.), of course if the corresponding OH abundance is known. For any assumed excitation temperature an 'abundance' may be derived that will scale the 'OH column densities' to total gas column densities.

From a correlation of W_{OH} with photographic extinction for the Taurus region (Wouterloot and Habing, 1984), we obtain an OH abundance of $\frac{N_{OH}}{N_H} = (12 \pm 3) \times 10^{-8}$, adopting $A_v = 0.75 A_{ph}$ and $N_H = 1.9 \times 10^{21} A_v$ (Spitzer, 1978; with $\frac{A_v}{E(B-V)} = 3.1$ and $N_H = N(HI) + 2.N(H_2)$). Indirectly, from a correlation with ^{13}CO column densities in L134 (Mattila et al., 1979) and assuming a ^{13}CO abundance of $(1.2 \pm 0.3) \times 10^{-6}$ (Taurus–Duvert et al., 1986), we derive $\frac{N_{OH}}{N_H} = (9 \pm 3) \times 10^{-8}$. The OH abundance in the Orion region results from the relationship found by Bloemen et al. (1984) between W_{CO} in Orion and the gamma ray emissivity measured by COSB. Adding the weak correlations found between W_{CO} and W_{OH} from our data, we derive an abundance of $\frac{N_{OH}}{N_H} = (7 \pm 3) \times 10^{-8}$.

In GMC214–13 the main line ratio tends to be near the optically thin limit. For this region we adopt $T_{ex}(1667) = 5.5$K and the value of $\frac{N_{OH}}{N_H} = (9 \pm 3) \times 10^{-8}$ to calculate masses and mean densities.

4. Results

Table 1 gives for a number of areas the adopted distance (d), the sum of the integrated line emission (W_{OH}), the main line ratio

Table 1. Parameters derived for clouds in Orion South and GMC214–13: the adopted distance, the sum of the integrated 1667 MHz line profiles, the mean main line ratio, a mass estimate from OH main line observations compared to those derived from ^{12}CO observations, mean density and mass per unit of length along the filaments.

Area:	d	ΣW_{OH}	$< \frac{Ta_{1665}}{Ta_{1667}} >$	M_{OH}	$M_{T_a(CO)}$	$M_{W_{CO}}$	n_H	mass/pc
	pc	K km/s			$10^4 M_\odot$		cm^{-3}	$\frac{10^3 M_\odot}{pc}$
Orion South	500	119	—	9	9.8	10.4	—	—
$209.5 < L < 210.0$	500	11	~ 1	~ 2.4	—	—	2000	5.5
$210.0 < L < 212.7$	500	39	0.87 ± 0.08	4.5	—	—	800	1.9
$212.7 < L < 215.5$	500	56	0.71 ± 0.04	~ 2.1	—	—	300	0.5
$215.5 < L < 217.5$	500	13	0.5 ± 0.2	0.8	—	—	250	0.3
NGC 2149	830	38	0.6 ± 0.1	6	4.4	4.4	200	0.7
L1646/1651	830	93	0.6 ± 0.1	15	12.2	8.6	350	0.8
L1652/South. Fil.	800	45	0.45 ± 0.05	7	3.2	2.5	250	0.6
Cl 216.5-7.5	800	21	0.5 ± 0.1	3	—	—	200	—
L1653, 54, 55, 56	1200	8	—	3	3.0	3.0	300	0.6
L1657	1200	> 5	—	>2	—	—	350	0.8

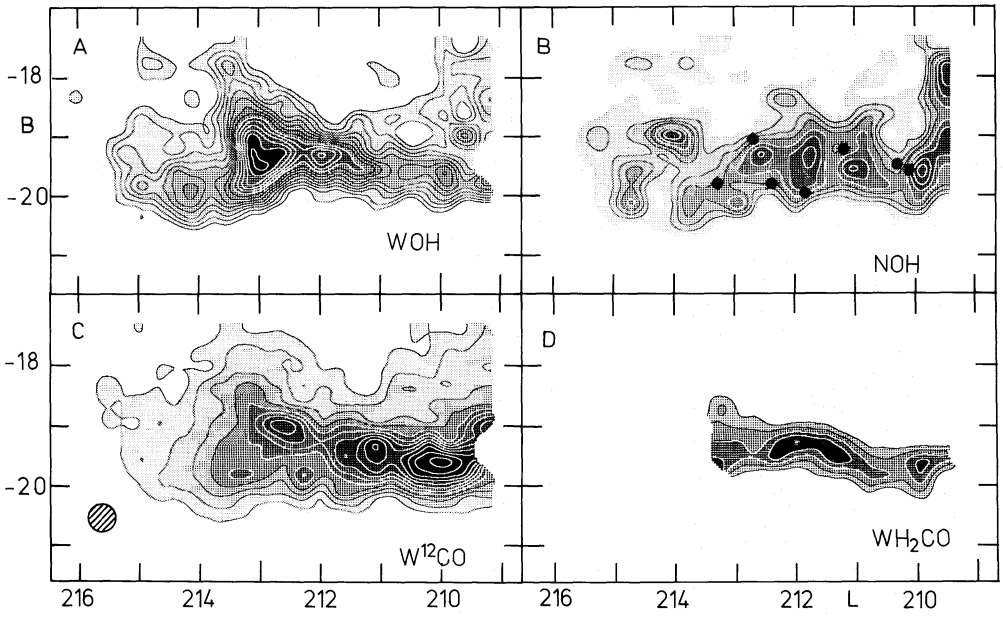

Fig. 6. A sequence of maps of different parameters for Orion South. **A)** W_{OH}, contour interval 0.1 K.km/s, lowest contour 0.3 K.km/s. **B)** N_{OH} (LTE), contour interval $20x10^{14} cm^{-2}$, lowest contour $40x10^{14}$, lowest nuance contour $20x10^{14}$. **C)** $W_{^{12}CO}$ (Maddalana et al., 1986), contour interval 2.0 K.km/s, lowest contour 2.0 K.km/s. **D)** W_{H_2CO} (Cohen et al., 1983), contour interval 0.2 K.km/s, lowest contour 0.4 K.km/s. Figures C) and D) are read off the published maps and are smoothed to the same beam and angular spacing as the *OH* data.

for the central part of the cloud, the total mass (Orion South, $L < 215.5$: LTE mass), the results from ^{12}CO observations (Maddalena et al., 1986), the mean density for an adopted effective depth of 10pc, and finally the mass per unit length along the filaments observed in the areas (see Sect. 4).

We find a total mass of all clouds in GMC214–13 of $2.9 \times 10^5 M_\odot$ and mean densities ranging from 200 to 350 cm^{-3}. The total mass estimates from *CO* data are $1.4 \times 10^5 M_\odot$ and $2.1 \times 10^5 M_\odot$, the latter from W_{CO} data, the first value by adding data on ^{13}CO and assuming LTE (Maddalena et al., 1986). The small systematic difference may be due to uncertainties in the adopted abundances. The mass distribution inferred from both observations however is significantly different. In *CO* the MonR2 area with many reflection nebulae is dominant, while in *OH* *L*1652 is more prominent.

Figure 6 shows both the *OH* column density (N_{OH}) map for Orion South, assuming LTE, and the distribution of W_{OH}. The main line ratio tends to increase for decreasing galactic longitude and latitude. This results in a strikingly different distribution of N_{OH} compared to W_{OH}. That the mass distribution probably is represented much better by N_{OH} than by W_{OH} follows from a comparison with ^{13}CO and H_2CO observations, which will be discussed below. This fact is an argument in favour for the LTE approach.

In Fig. 6 we also show W_{H_2CO} data from Cohen et al. (1983) and $W_{^{12}CO}$ data from Maddalena et al. (1986). The data were read off the published maps and smoothed in such a way that the resolution is comparable to our *OH* data. The ^{13}CO data have such high resolution and detailed structure that smoothing is inaccurate unless done from the original data. The W_{H_2CO} data show excellent agreement with the $W_{^{13}CO}$ data of Bally et al. (1987). The following features are present in both maps.

1) Matter near M42, not contained in our maps, is distributed in a clumpy ∫–shaped ridge between $L = 208^o.7$ and $L = 209^o.9$. Near $L = 209^o.6$ the ridge is at $B = -19^o.6$ and molecular gas is at radial velocities between 6 and 10 km/s. The ridge contains extremely dense clumps ($n_H > 10^6 cm^{-3}$, e.g. Batrla et al., 1983) and is the area of massive star formation.

2) At $L = 210^o.1$, $B = -19^o.5$ there is an extension of the ridge in H_2CO, that is seen in the high resolution ^{13}CO data as a separate cloud clump at 6–7 km/s (Bally et al., 1987; Fig. 2).

3) At $L = 210^o.4$, $B = -19^o.7$ there is an enhancement of both W_{H_2CO} absorption and $W_{^{13}CO}$ emission, which is part of an extended very clumpy filament. Its gas is seen at $V_r = +7$ km/s. This filament forms the low latitude part of the *A*–shaped structure that is interpreted by Bally et al. as resulting from the refraction of shocks at the dense ridge. Its highly clumpy and filamentary structure makes an origin by a shock likely.

4) The high latitude part of the *A* is formed by gas at $L = 210^o.9$, $B = -19^o.3$; $L = 211^o.7$, $B = -19^o.2$ and $L = 212^o.3$, $B = -19^o.3$, at velocities of 4–5 km/s, that has a well defined high latitude edge. The gas itself seems to be less clumpy than seen in the ridge of feature 3. This gas is the dominant feature in the W_{H_2CO} map, seen as a banana–shaped ridge in Fig. 5.

5) At $L = 212^o.5$, $B = -19^o.0$ a peak in ^{13}CO is seen with a weak counterpart in the H_2CO map. $W_{^{12}CO}$ shows a strong peak at this position, coinciding with a few reflection nebulae (VdB 55). Judging from the POSS plates these reflection nebulae are at the edge of the dust cloud.

6) At $L = 212^o.8$ there is a gap in the distribution of molecular material, south of which weak extended ^{13}CO emission and H_2CO absorption is observed. This is part of another cloud, called L1647.

An important difference between the ^{13}CO and H_2CO results is that the ridge (feature 1) is dominant in ^{13}CO whereas feature 4 is dominant in H_2CO absorption.

Several features in the N_{OH} map are probably real indications of mass. The banana–shaped ridge is present (feature 4). The onset of the ridge is visible (feature 2) and there is an enhancement at $L = 210^o.5$, $B = -19^o.8$ that is identified as feature 3. False peaks may be those at $L = 209^o.6$, $B = -18^o$ and $L = 214^o.0$, $B = -19^o.0$ where at several adjacent positions high main line ratios are found. These may not be significant, because the *OH* emission is rather weak here, individual main line ratios are of the order of 0.9 ± 0.2, and there is no ^{12}CO counterpart (H_2CO

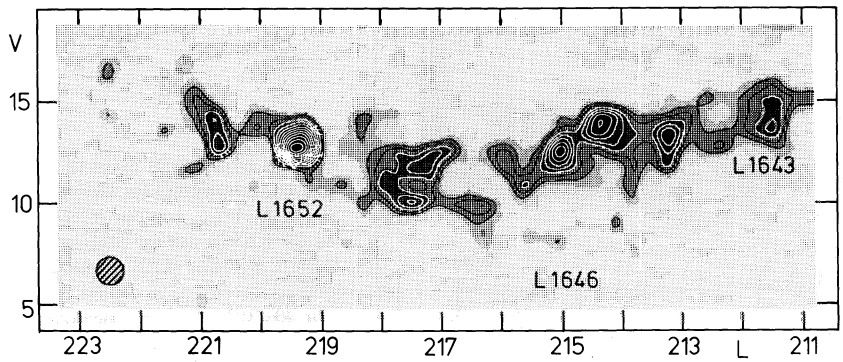

Fig. 7. $L-V$ map of spectra sampled along the filament running from L1643 to the cloud at $L = 222.5, B = -5$, following the peak of the filament that is seen in W_{OH} (Fig. 4b). Weak velocity gradients are present. Contour values: (0.06), 0.08, 0.10, 0.12, ... K.

and ^{13}CO observations are not available). No attempt was made to remove such spurious peaks from the map, because the peak at $L = 209^o.6$ coincides with the location of a number of point sources in the IRAS Point Source Catalogue and the peak at $L = 214^o$ coincides with an area of unusual IRAS colours. This may warrant further study of these places.

Surprisingly peaks in the ^{12}CO distribution, as shown with black dots in the N_{OH} map of Fig. 5, are found at depressions or steep gradients in OH column density. There is a pronounced displacement between the OH peak at $L = 212^o.7$, $B = -19^o.3$ and the CO peak at $L = 212^o.7$, $B = -19^o.0$. It is possible that the OH abundance is less at such "warm" spots (as found from gas–phase chemistry modelling of dense molecular clouds, Herbst and Leung, 1986), but as ^{12}CO is optically thick, contrary to OH, it is more likely that these peaks in CO coincide with peaks in local kinetic temperature. We therefore conclude that the warm spots are found dominantly at the edges of the clouds where they are due to reflection nebulae.

The area with $T_a(1667) > 0.1$K, without the suspect peaks at $L = 209^o.6$ and $L = 214^o.0$, has an integrated column density $\Sigma\ N_{OH} = 8.0 \times 10^{17} cm^{-2}$. From an OH abundance of $(7 \pm 2) \times 10^{-7}$ the total mass of the surveyed part of Orion South is $9 \pm 2 \times 10^4 M_\odot$. Including the areas that are outside our map, the total mass of Orion South will be about $10 \pm 3 \times 10^4 M_\odot$. This value is in good agreement with mass estimates by other means: $10 \times 10^4 M_\odot$ ($^{13}CO/^{12}CO$, $W^{12}CO$; Maddalena et al., 1986) and $(12 \pm 4) \times 10^4 M_\odot$ (gamma ray emissivity; Caraveo et al., 1980). Only about two thirds of Orion South has been observed in H_2CO (Cohen et al., 1983) and ^{13}CO (Bally et al., 1987) which both give a mass estimate of $5x10^4 M_\odot$.

The low OH column densities for $L < 212^o.7$ imply a decreasing mean density, all the way down to diffuse cloud densities. Close to the massive star forming region, near $L = 209^o.6$, the volume averaged density is about $2x10^3 cm^{-3}$ assuming an effective depth of 10pc. To the south, between $L = 210^o.3$ and $L = 212^o.7$, the mean density is about $800 cm^{-3}$. Further south, between $L = 212^o.7$ and $L = 215^o.0$, it is only about $350 cm^{-3}$, similar to the values found for the clouds of GMC214–13.

5. Velocity and spatial structure

The maps of Figs. 4 show that both giant molecular complexes have similar spatial structure. The molecular gas is located in extended filaments or ridges (Morris et al., 1980) that form parts of ring like structures. Such filaments are seen in other molecular clouds also, like Taurus (e.g. Duvert et al., 1986) and Ophiuchus (e.g. Wouterloot, 1984a; De Geus, 1988).

5.1. The Monoceros region

The main GMC214-13 filament goes from $L = 211^o$ in L1643 south along L1646, L1651 and L1652 until $L = 221$, possibly extending down to the cloud at $L = 222^o.5$, $B = -5^o$. The latter part was called the "Southern Filament" by Thaddeus (1982). The filament has a minimum (projected) size of 160pc. In Fig. 7 the distribution of emission along this filament in velocity space is shown. The sequence of spectra in the L–V map follow the peaks in emission of the filament in Fig. 4b. There is a smooth projected velocity gradient of -0.037 ± 0.008 km/s.pc between $L = 211$ and $L = 218$, and possibly an opposite gradient of $+0.04 \pm 0.01$ between $L = 218$ and $L = 223$. The standard deviation of the scatter in velocities around this gradient is 1.3 km/s for individual peaks in the OH emission. The absolute velocity range is about 8 km/s.

Figure 7 may be interpreted differently: the velocity is constant between $L = 215^o.5$ and $L = 211^o$ and deviates between $L = 215^o.5$ and $L = 220^o$. The clouds that have deviating radial velocities appear to lie on a circular structure around $L = 216.8$, $B = -10.1$ with a radius of 47 ± 7 pc (see Fig. 3b, the peak antenna temperature map and also Fig. 4a where this ring is visible from the positions of clouds with low radial velocities, $V_r < 8.6$ km/s). The "relaxed" gas at $L < 215.5$ has a radial velocity of 13.6 km/s and if it follows the general differential galactic rotation, these clouds should be at a distance of 1060 ± 90 pc (from the average local values of $\Theta = 222$ km/s and $R = 8.5$ kpc; Kerr and Lynden–Bell, 1986). This is more distant than the 830pc found for MonR2. At $L = 216.0$, $B = -10.1$ there is a small open cluster, NGC2215, believed to be at a distance of about 1000pc (Becker, 1960) that may represent an earlier episode of star formation in the region (Downes et al., 1975). It is, however, a poor cluster with only 33 stars brighter than $M_v = +4^m$ and only about 2.9pc in diameter (Becker, 1960). There is no H_α emission in the map of Sivan (1974) that can be associated with such a ring. There are no known associated O and B stars in the ring, though some stars of MonR2 may be at the outer edge.

5.2. The Orion region

The bulk matter in Orion South is also found in a big filament, running from $L = 208^o$ along the $\int$–shaped ridge of OMC1, along the banana-shaped ridge between $L = 211^o$ and $212^o.7$ and then splits with a part running south, containing L1647 and the clouds near $L = 217^o$, $B = -17^o$, and another branch bending east to $L = 213^o.8$, $B = -17^o.8$. There is a velocity gradient along

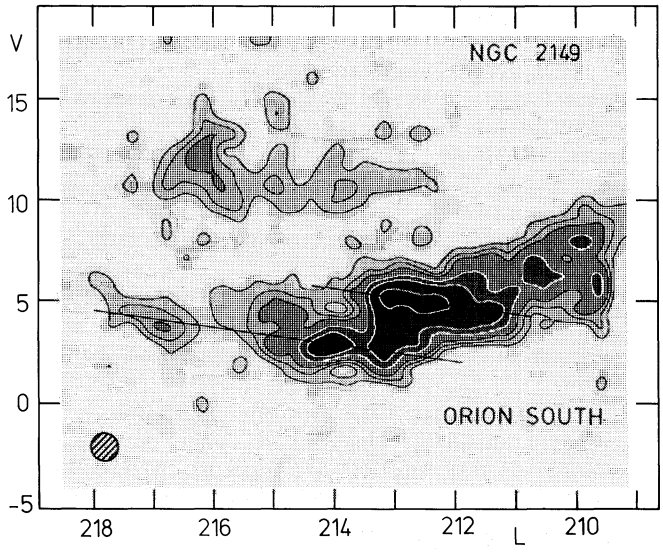

Fig. 8. $L-V$ map of the peak antenna temperature of 1667 MHz, searched for in the interval $-21 < B < -14.7$, within the region surveyed. Full drawn lines show the velocity gradients along the eastern and southern filament in Orion South. The clouds at $V_{lsr} = +10$ km/s are part of GMC214–13 (NGC2149). Contour values: (0.06) 0.08, 0.12, 0.16, 0.24, 0.32, 0.48 K.

each of these branches, in projection $+0.03 \pm 0.01$ km/s.pc for the eastern branch and $+0.036 \pm 0.006$ for the southern branch. The velocity gradients have the opposite sign from the well known general velocity gradient observed in Orion South with a magnitude of -0.14 ± 0.03 km/s.pc. Figure 8 is an alternative L–V plot. For each (L,V) the peak antenna temperature is given for the range $-14.7 > B > -21.0$. Both filaments show up in this L–V diagram as separate structures (indicated with full drawn lines).

At $V_r = 11$ km/s there is emission associated with NGC2149, well separated from the clouds of Orion South. The velocity gradient in the filaments may be interpreted as resulting from an infall of matter on the bulk mass at $L = 211^o$. If the cloud is about parallel to direction in which the OB cluster is elongated, it is facing away from the observer. Infalling matter is seen at negative velocities, with more negative values as the gas comes closer to the main cloud. In Sect. 3.2 it was found that this gas has low (diffuse cloud) mean densities.

This scenario fails to explain the high radial velocities in the cone area, for $L < 212.7$. Here the clouds have much higher radial velocities than expected from the local galactic rotation velocity field (+10 versus +5 km/s). Therefore if this difference is not caused by some random motion, then the gas in the main filament is pushed away from us and from the cluster. Possibly by shocks, cloud evaporation (rocket effect) or a pressure disequilibrium due to local heating of the bubble gas (see Chiang and Prendergast, 1985), all having their source of energy in the nearby OB association. The mass per unit length along the filament as found from the OH observations is not constant, but tends to be higher north of $L = 212.7$ than south of it (see Table 1). This also points to a displacement (compression) of matter along the axis of the cloud, away from the OB association. A similar process acts on the Orion North cloud too, where the gas nearest to the association has similar high radial velocities (Goss et al., 1976, Maddalena et al., 1986).

6. Conclusions

An LTE interpretation of the OH main line observations appears to give reliable mass estimates and a reasonable picture of the mass distribution within a giant molecular cloud as compared to the results of other optically thin molecular transitions (^{13}CO, H_2CO).

In GMC214–13 (Monoceros R2, L1652) matter is distributed in ridges or filaments that have weak projected velocity gradients of the order of ± 0.04 km/s.pc and a total mass of $3 \pm 1 \times 10^5 M_\odot$. The total mass is typical for a GMC and similar to that of GMC209–13 (Orion South and Orion North). Compared to GMC209–13 however matter is found in a larger volume of space and has relatively low mean densities.

Similar low mean densities, spatial and velocity structure as found in GMC214–13 are seen in the most southern part of Orion South in the area that is outside the HI shell associated with the Barnard Loop. Inside that HI shell the influence of the OB association is notable. Approaching the area of massive star formation in the top of the cloud, near M42, the mean density and total mass per unit length along the filament increases. This and the high radial velocities found in the top of Orion South (and in Orion North) indicate that large amounts of mass are forced to move away from the OB association.

The total mass of Orion South is $1.0 \pm 0.3 \times 10^5 M_\odot$. The mass is distributed in similar filaments as in GMC214–13. The mass distribution found differs from that derived from $W_{^{12}CO}$. The OH column density tends to be low at peaks in the CO emission. Because such peaks coincide with reflection nebulae and HII regions, this can imply that in Orion South such objects are found preferentially at the outer edges of the cloud.

The high efficiency of massive starformation in the Orion region with respect to that in the Monoceros region may result from the influence of pre–existing massive stars and from the favourable orientation of the Orion South filament with respect to the cluster of stars.

Acknowledgements. We thank the staff of the Dwingeloo radio observatory, in particular J. Tenkink, D. Moorrees and H. Lem, and J.H. Burger and G.F. Rhee for assistance during the observations. We thank P. te Lintel Hekkert for supporting the POPS–LYNCAL package. This work was initiated by H.J. Habing and gained by fruitful discussions with A. Blaauw and P. Maloney. The Dwingeloo telescope is operated by the Netherlands Foundation for Radio Astronomy.

References

Andresen P., Häusler D., Lülf H.W., Kegel W.H.: 1984, *Astron. Astrophys.* **138**, L17
Andresen P.: 1986, *Astron. Astrophys.* **154**, 42
Bally J., Langer W.D., Stark A.A., Wilson R.W.: 1987, *Astrophys. J. Lett.* **312**, L45
Baud B., Wouterloot J.G.A.: 1980, *Astron. Astrophys.* **90**, 297
Batrla W., Wilson T.L., Bastien P., Ruf K.: 1983, *Astron. Astrophys.* **128**, 279
Becker W.: 1960, *Z. Astrophys.* **49**, 168
Beichman C.A.: 1986, in *Light on Dark Matter*, ed. F.P. Israel, Reidel, Dordrecht, p. 279
Bertojo M., Cheung A.C., Townes C.H.: 1976, *Astrophys. J.* **208**, 914

Bouloy D., Omont A.: 1977, *Astron. Astrophys.* **61**, 405
Bujarrabal V., Nguyen-Q-Rieu: 1980, *Astron. Astrophys.* **91**, 283
Caraveo P.A., Bennett K., Bignami G.F., Hermsen W., Kanbach G., Lebrun F., Masnou J.L., Mayer–Hasselwander H.A., Paul J.A., Sacco B., Scarsi L., Strong A.W., Swanenburg B.N., Wills R.D.: 1980, *Astron. Astrophys.* **91**, L3
Castor J., McCray R., Weaver R.: 1975, *Astrophys. J. Lett.* **200**, L107
Chiang W.H., Prendergast K.H.: 1985, *Astrophys. J.* **297**, 507
Cohen R.J., Matthews N., Few R.W., Booth R.S.: 1983, *Monthly Notices Roy. Astron. Soc.* **203**, 1123
Cowie L.L., Songaila A., York D.G.: 1979, *Astrophys. J.* **230**, 469
Crutcher R.M.: 1977, *Astrophys. J.* **216**, 308
Crutcher R.M.: 1979, *Astrophys. J.* **234**, 881
De Geus E.J.: 1988, *Stars and Interstellar Matter in Scorpio Centaurus*, Ph D thesis, Leiden University, p. 41
Dickey J.M., Crovisier J., Kazès I.: 1981, *Astron. Astrophys.* **98**, 271
Dixon R.N., Field D.: 1979, *Monthly Notices Roy. Astron. Soc.* **189**, 583
Downes D., Winnberg A., Goss W.M., Johansson L.E.B.: 1975, *Astron. Astrophys.* **44**, 243
Downes D., Genzel R., Becklin E.E., Wynn–Williams C.G.: 1981, *Astrophys. J.* **244**, 869
Duvert G., Cernicharo J., Baudry A.: 1986, *Astron. Astrophys.* **164**, 349
Few R.W., Booth R.S.: 1979, *Monthly Notices Roy. Astron. Soc.* **188**, 181
Field G.B., Goldsmith D.W. and Habing H.J.: 1969, *Astrophys. J. Lett.* **155**, L149
Flower D.R.: 1980, *Astron. Astrophys.* **83**, 33
Goss W.M.: 1968, *Astrophys. J. Suppl. Ser.* **15**, 131
Guibert J., Elitzur M., Nguyen-Q-Rieu: 1978, *Astron. Astrophys.* **66**, 395
Heiles C., Habing H.J.: 1974, *Astron. Astrophys. Suppl. Ser.* **14**, 1
Herbst E., Leung C.M.: 1986, *Monthly Notices Roy. Astron. Soc.* **222**, 689
Herbst W., Racine R.: 1976, *Astron. J.* **81**, 840
Iben I., Talbot R.J.: 1966, *Astrophys. J.* **144**, 968
Israel F.P. (ed.): 1986, *Light on Dark Matter*, Reidel, Dordrecht, p. 280
Jenniskens P.M.M., Habing H.J., Wouterloot J.G.A., Te Lintel Hekkert P., Blaauw A.: 1986, in *Light on Dark Matter*, ed. F.P. Israel, Reidel, Dordrecht, p. 325
Jenniskens P.M.M.: 1988, *Factor Twee*, Internal research note, Leiden Observatory.
Kaplan H., Shapiro M.: 1979, *Astrophys. J. Lett.* **229**, L91
Kerr F.J., Lynden–Bell D.: 1986, *Monthly Notices Roy. Astron. Soc.* **221**, 1023
Kutner M.L., Tucker K.D., Chin G., Thaddeus P.: 1977, *Astrophys. J.* **215**, 521
Maddalena R.J., Morris M., Moscowitz J., Thaddeus P.: 1986, *Astrophys. J.* **303**, 375
Mattila K., Winnberg A., Grasshoff M.: 1979, *Astron. Astrophys.* **78**, 275
McKee C.F., Ostriker J.P.: 1977, *Astrophys. J.* **218**, 148
Morris M., Montani J., Thaddeus P.: 1980, in *Interstellar Molecules*, ed. B.H. Andrew, IAU Symp. **87**, 197
Parsamian E.S., Chavira E.: 1982, *Boletin del Instituto de Tonantzintla* **3**, 69
Racine R.: 1968, *Astron. J.* **73**, 233
Reynolds R.J., Ogden P.M.: 1979, *Astrophys. J.* **229**, 942
Spitzer L.: 1978, *Physical Processes in the Interstellar Medium*, Wiley, New York, p. 3
Strom K.M., Strom S.E., Carrasco L., Vrba F.J.: 1975, *Astrophys. J.* **196**, 489
Thaddeus P.: 1982, in *Symposium on the Orion Nebula to honour Henry Draper*, eds. A.E. Glassgold, P.J. Huggins, E.L. Schucking, N.Y. Aca. of Sci. Publ. **395**, 9
Turner B.E., Heiles C.E.: 1974, *Astrophys. J.* **194**, 525
Van den Bergh S.: 1966, *Astron. J.* **71**, 990
Weaver H., Williams D.R.W.: 1974, *Astron. Astrophys. Suppl. Ser.* **17**, 251
Wouterloot J.G.A., Habing H.J.: 1984, *Astron. Astrophys. Suppl. Ser.* **60**, 43
Wouterloot J.G.A.: 1984a, *Astron. Astrophys.* **134**, 244
Wouterloot J.G.A.: 1984b, *Astron. Astrophys.* **135**, 32
Zeng Q., Sun J., Lou G.F.: 1987, *Astron. Astrophys.* **172**, 299

This article was processed by the author using Springer-Verlag TEX AA macro package 1989.